Advanced Engineering Materials

Micro-Embossing Formability of a Superlight Dual-Phase Mg-Li Alloy Processed by High-Pressure Torsion **

--Manuscript Draft--

Manuscript Number:	
Full Title:	Micro-Embossing Formability of a Superlight Dual-Phase Mg-Li Alloy Processed by High-Pressure Torsion **
Article Type:	Full Paper
Section/Category:	
Keywords:	dual-phase microsructures; high-pressure torsion; Mg-Li alloy; micro-embossing; micro-forming.
Corresponding Author:	Bin Guo Harbin Institute of Technology CHINA
Additional Information:	
Question	**Response**
Please submit a plain text version of your cover letter here.	Dear Editors, Uploaded please find one original manuscript entitled “Micro-embossing formability of a superlight dual-phase Mg-Li alloy processed by high-pressure torsion”, for review towards publication in Advanced Engineering Materials. The paper is original and unpublished and is not being considered for publication elsewhere. Our main justification for submitting this work as an article is: (1) The interactive effects of the cavity widths of the female die and dual phases on the formability of micro-embossing were analyzed, and the results show a UFG Mg-Li alloy reduces the adverse effects of dual phases on the formability of micro-embossing. (2) The co-existence of the α and β phases influences the deformation processing of micro-embossing. This paper gives the deformation mechanism of micro-embossing in the dual-phase Mg-Li alloy. (3) This paper demonstrates that the UFG alloy processed by HPT has a very good potential for applications in micro-forming. Thank you for your time on our manuscript. Sincerely yours, Bin Guo
Do you or any of your co-authors have a conflict of interest to declare?	No. The authors declare no conflict of interest.
Corresponding Author Secondary Information:	
Corresponding Author's Institution:	Harbin Institute of Technology
Corresponding Author's Secondary Institution:	
First Author:	Jie Xu
First Author Secondary Information:	
Order of Authors:	Jie Xu
	Qian Su
	Chenxi Wang
	Xinwei Wang

	Debin Shan
	Bin Guo
	Terence G. Langdon
Order of Authors Secondary Information:	
Abstract:	Micro-embossing tests were performed on a coarse-grained (CG) and an ultrafine-grained (UFG) dual-phase Mg-Li alloy processed by high-pressure torsion (HPT) using different widths of the female die at ambient temperature under a force of 9 kN. The surface topography, rib profiles and microstructures of the cross-sections were measured by scanning electron microscopy, confocal scanning laser microscopy and optical microscopy, respectively. The interactive effects of the cavity widths of the female die and dual phases on the formability of micro-embossing were analyzed. Numerical simulations were performed to study the effects of the dual-phases on the filling behavior of the CG and UFG alloys. The results show a UFG Mg-Li alloy reduces the adverse effects of dual phases on the formability of micro-embossing. Micro-channel arrays with channel widths ranging from 50 to 200 μm were fabricated with good geometrical accuracy using a UFG dual-phase alloy at ambient temperature, thereby establishing the excellent potential for using UFG dual-phase Mg-Li alloys processed by HPT for applications in micro-forming.

DOI: 10.1002/adem.((please add manuscript number))

Micro-Embossing Formability of a Superlight Dual-Phase Mg-Li Alloy Processed by High-Pressure Torsion **

By *Jie Xu, Qian Su, Chenxi Wang, Xinwei Wang, Debin Shan, Bin Guo** and *Terence G. Langdon*

[*] *Prof. B. Guo, J. Xu, Q. Su, X. W. Wang*
Key Laboratory of Micro-systems and Micro-structures Manufacturing of Ministry of Education
Harbin Institute of Technology, Harbin150080, China
E-mail: guobin@hit.edu.cn
C. X. Wang, Prof. D. B. Shan
National Key Laboratory for Precision Hot Processing of Metals, Harbin Institute of Technology
Harbin Institute of Technology, Harbin150080, China
Prof. T. G. Langdon
Materials Research Group, Department of Mechanical Engineering,
University of Southampton, Southampton SO17 1BJ, UK
Departments of Aerospace & Mechanical Engineering and Materials Science,
University of Southern California, Los Angeles CA 90089-1453, USA

Micro-embossing tests were performed on a coarse-grained (CG) and an ultrafine-grained (UFG) dual-phase Mg-Li alloy processed by high-pressure torsion (HPT) using different widths of the female die at ambient temperature under a force of 9 kN. The surface topography, rib profiles and microstructures of the cross-sections were measured by scanning electron microscopy, confocal scanning laser microscopy and optical microscopy, respectively. The interactive effects of the cavity widths of the female die and dual phases on the formability of micro-embossing were analyzed. Numerical simulations were performed to study the effects of the dual-phases on the filling behavior of the CG and UFG alloys. The results show a UFG Mg-Li alloy reduces the adverse effects of dual phases on the formability of micro-embossing. Micro-channel arrays with channel widths ranging from 50 to 200 μm were fabricated with good geometrical accuracy using a UFG dual-phase alloy at ambient

temperature, thereby establishing the excellent potential for using UFG dual-phase Mg-Li alloys processed by HPT for applications in micro-forming.

1. Introduction

With the rapid development of product miniaturization in the application of micro-electro-mechanical systems (MEMS), micro-forming has attracted considerable attention in recent years. Products with micro-array channels have potential applications in the fields of micro-fluids, micro-optics and medical and biological devices.[1-3] The micro-embossing process is a promising procedure for producing micro-array structures due to its excellent capabilities such as low cost, high efficiency and large scale and well-structured fabrication.[4] Twenty years ago, a micro-embossing technique to fabricate metallic microstructures using a silicon die were developed and in later research a pure coarse-grained (CG) Al micro-optical grating was manufactured by a high precision cold embossing method using a silicon die.[5, 6] The micro-array channels in this research exhibited non-flat planks with ridges. Furthermore, straight micro-channels and micro-complex structures were fabricated by cold and superplastic micro-embossing with a silicon die.[7] Meanwhile, direct micro-embossing to fabricate micro-array channels in conventional CG Al at room temperature was proposed and the micro-embossing process with an ultrafine-grained (UFG) pure aluminum was studied and used this material to fabricate micro-array channels for MEMS components.[1, 8] Subsequently, the hot micro-embossing process of micro-array channels in UFG pure Al using an automatic balance device was investigated.[9]

Despite these fairly extensive investigations, size effects may occur and appear to be important in controlling the material deformation behavior when the feature sizes, such as the

grain size and the specimen size, are reduced to the micro/meso scale.[10-14] Extensive work has been reported studying the effects of grain size and geometric size on plastic deformation in different micro-embossing processes. For example, using experiments and simulations, the effects of grain and geometric sizes on the coining process was revealed and results showed that certain preform shapes can enhance the feature formation by allowing a favorable flow of the bulk material.[15, 16] Meanwhile, researchers found that the surface roughness increases with strain and the variation rate increases with grain size during micro-embossing of micro-channels and the influence of die cavity dimension on the formability in the warm coining process which revealed that the formability decreases with an increase of the ratio of the grain size to the die cavity width.[17, 18] Furthermore, a multi-region model which considered the grain orientation and boundary by the micro-coining process was proposed in order to investigate the size effects of micro-bulk formation and the grain and geometry size effects on deformation in roll-to-plate micro/meso-imprinting of pure copper was investigated.[19, 20] Nevertheless, a comprehensive examination of these reports shows that there is little or no information on the interactive effects of the cavity width of a female die and the presence of dual phases on the formability in micro-embossing.

The Mg-Li alloys are known as some of the lightest metals in the engineering field and they are attracting significant interest in both scientific research and in industrial applications such as in the aerospace, military and electronic sectors due to their important properties such as a lowest density as a structural metallic material, a high specific stiffness, a good magnetic screening, excellent cold formability and an exceptional damping capacity.[21-26] According to the Mg-Li binary phase diagram, Mg-Li alloy can have a dual-phase microstructure depending on the amount of Li in Mg.[27] Thus, Mg-Li alloys with Li content between 5.5 and

10.2 wt. % consist of an Mg-rich hexagonal-close-packed (hcp) structured solid solution (α phase) and a Li-rich body-centered-cubic (bcc) structured solid solution (β phase). These co-existing dual-phases lead to an interesting compromise of moderate strength and excellent ductility by comparison with the single α or β phase alloys.[28] Another advantage of fine-grained Mg-Li alloys with an α phase and a β phase is that they exhibit superplasticity at elevated temperatures.[29] For example, when the microstructure is refined to ultrafine grains by equal-channel angular pressing (ECAP), it was shown that the alloys are capable of exhibiting superplasticity with tensile elongations at 473 K up to ~970% or ~1780%.[30, 31] Additionally, a UFG Mg-8%Li alloy fabricated by high-pressure torsion (HPT) showed low temperature superplasticity having elongations of >400% at temperatures above 323 K and a later report documented an elongation of 440% at room temperature.[32, 33] Based on the conclusions from these and earlier studies, it is suggested that UFG dual-phase Mg-Li alloys should have a strong potential for use in all forms of micro-forming applications.[34, 35]

In the present research, micro-embossing tests were conducted on a dual-phase Mg-Li alloy having two different average grain sizes using different cavity widths for the female die under a selected embossing force at ambient temperature. In addition, finite element simulations were adopted to examine the micro-embossing of the dual-phase Mg-Li alloy in order to provide a comprehensive analysis of the experimental results. Thus, the interactive effects of the cavity width of the female die and the dual phases on the formability of micro-embossing were carefully analyzed based both on experimental results and numerical simulations.

2. Experimental material and procedures

2.1. Preparation of UFG Mg-Li alloy by HPT

An Mg-9% Li-1% Zn (in wt. %) alloy was received in the form of an extruded plate with a thickness of 20 mm. The microstructure of the as-received alloy is shown in **Figure 1**a and at a higher magnification in **Figure 1**b where it is apparent that the structure contains a co-existence of the α and β phases. The volume fractions of the α and β phases were determined by an image analyzer as ~ 63% and ~ 37%, respectively. The average value of the width of the α and β phase cell perpendicular to the extrusion direction was estimated as ~22 μm.

To prepare specimens for HPT processing, discs were machined from the plate with diameters of ~9.8 mm and thicknesses of ~1.0 mm and these discs were then carefully ground and polished on both sides to final thicknesses of ~0.82 mm. For the HPT processing (**Figure 2**a), each disc was placed in a depression on the lower anvil and then the two anvils were brought together to impose an applied pressure, P, of 6.0 GPa. The torsional straining was achieved through rotation of the lower anvil using a rotation rate of 1 rpm. All discs were processed at room temperature through 5 revolutions under quasi-constrained conditions where there is some limited outflow of material around the periphery of the disc during the torsional straining.[36]

The phase distributions of the dual-phase Mg-Li alloy processed by HPT were observed by backscattered electron imaging in a scanning electron microscope (SEM). The results (**Figure 2**b) show that the α phases are broken up and this generates a large number of α phase 5 particles which become dispersed in the β phases (**Figure 2**c). The microstructure was also observed by transmission electron microscopy (TEM) and the results in **Figure 2**d and **Figure 2**e show that a UFG Mg-Li alloy was achieved by HPT processing with an average grain size of ~290 nm and with a high fraction of high-angle boundaries.

The mechanical properties were measured using Vickers microhardness and micro-tensile testing. The microhardness of the as received dual-phase Mg-Li alloy was measured on areas of α and β phases and the average hardness values, Hv, were recorded as ~47.7 and ~44.1, respectively. After HPT processing, the average hardness value, Hv, of the UFG Mg-Li alloy was ~63.4 and this increase in hardness shows that the mechanical properties may be significantly improved by HPT processing. Curves of true stress and true stain for both the as-received and the UFG Mg-Li alloy are shown in **Figure 3**. These curves show that the saturation strength of the dual-phase Mg-Li alloy is significantly improved from ~175 MPa to ~240 MPa though HPT processing and this is consistent with the hardness measurements.

The mechanical property parameters for the α and β phases can be calculated from the true stress-true strain curves of the as-received Mg-Li alloy based on a mixing strength model developed for long fiber composite materials written by

$$\sigma_{AR} = \sigma_{\alpha} V_{\alpha} + \sigma_{\beta}(1 - V_{\alpha}) \quad (1)$$

where σ_{AR} is the flow stress of the as-received alloy, σ_{α} is flow stress of α phase, σ_{β} is flow stress of β phase and V_{α} is relative content of α phase. As the strength and hardness of the material are generally considered to hold a proportional relationship, the ratio of the two phase strengths may be obtained by the ratio of the two phase hardnesses. Thus, the relationship of two phase strength can be expressed as

Using this approach, the true stress and true strain curves of the two individual phases can be calculated as shown in **Figure 3** where these results may be used as the mechanical parameters of plastic deformation for the two separate phases.

2.2 The micro-embossing tool and parameters

The micro-embossing tool was designed with split female dies which were fabricated by micro-grinding with both high dimensional accuracy and surface quality as shown in **Figure 4**a. Five different sizes of female micro dies, with widths, *w*, of 25, 50, 100, 150 and 200 μm and the same ratio of height to width of $h/w = 3$ were adopted in the tests as shown in **Figure 4**b. The micro-embossing samples were machined from the HPT discs by electro-discharge machining to produce small blocks with dimensions of 5.5 (length) × 3.5 (width) mm^2 as shown in **Figure 4**c. Before the micro-embossing tests, the specimens were mounted, ground on SiC papers in series to 4000 and then mechanically polished until a mirror-like surface was achieved. The micro-embossing tests were conducted on the CG and UFG Mg-Li alloy plate with a maximum force, *F*, of 9 kN at a loading rate of 1.0 μm s^{-1} at ambient temperature with a Zwick/Roll Z010 testing machine. To reduce the influence of friction, the contact surfaces with the specimens were lubricated with castor oil so that the micro-compression tests were conducted in well-lubricated conditions.[37] The surface quality of the embossed rib after micro-embossing was examined using an FEI Quanta 200FEG field emission SEM and the heights of the micro-ribs were measured using a confocal scanning laser microscope (Olympus Co., OLS3000). In addition, to evaluate the filling behavior during micro-embossing, the microstructures of the ribs in the cross-sections were observed by optical microscopy (OM). Thus, the micro-embossing test of the micro-array channels was conducted in order to evaluate the potential for using the UFG Mg-Li alloy for future micro-forming applications.

2.3 Finite element modeling (FEM) of micro-embossing in Mg-Li alloy

Finite element simulations were adopted to reveal the filling behavior of the micro-embossing by ABAQUS. In this work, the Voronoi method was used to generate the grain structures for simulating the filling behavior of the α and β phases in the rib region of the die for the as-received Mg-Li alloy. The nuclei were seeded by the function of rand in the software Matlab where the function of rand can generate pseudo-random numbers with uniform distributions. A virtual geometrical morphology of grains was created by the function of Voronoi in Matlab. Through the software interface, a geometric model was read into ABAQUS/CAE using python, the script language of ABAQUS. In order to study the effect of the different dual-phase strengths on the forming process, some grains of the Voronoi grain geometry model were given material properties of the α phase and the others were given material properties of the β phase according to the original distributions of the two phases in the Mg-Li alloy. It was assumed that the properties of the material were isotropic in the grain and non-grain regions of the finite element model and the same plastic properties were assigned to the grain region from grains to grains. The plastic properties of each grain were assumed to be the same and for the UFG Mg-Li alloy the FEM model was considered as a uniform continuum using CPE4R element type. Based on these conditions, the finite element models of micro-embossing were established as shown schematically in **Figure 5** for the as-received alloy and the UFG Mg-Li alloy, respectively.

3. Experimental results

3.1 The filling height of micro-embossing in the dual-phase Mg-Li alloy

Figure 6 plots the filling height of the rib after micro-embossing of the as-received and UFG dual-phase Mg-Li alloy processed by HPT with channel widths ranging from 25 to 200 μm

under a maximum force of 9 kN at room temperature. It is readily apparent that the filling height of the embossed specimens increases with increasing channel width for both the CG and the UFG dual-phase alloy. The height of the embossed rib increases from ~23 to ~102 μm when the channel width changes from 25 to 200 μm for the CG dual-phase alloy whereas the corresponding heights for the UFG dual-phase alloy increase only from ~20 to ~55 μm over the same range of the dimensional changes of the die. Thus, there is an increasing filling rate for the CG specimens compared with the UFG dual-phase Mg-Li alloy and furthermore, for any selected channel width, the filling heights of the CG samples are higher than for the UFG alloy. These results show that the UFG dual-phase alloy shows no improvement in terms of formability for micro-embossing under the same maximum force at ambient temperature.

3.2 Surface topography after micro-embossing in the dual-phase Mg-Li alloy

The surface topographies of the ribs after micro-embossing of the as-received dual-phase Mg-Li alloy are shown in **Figure 7** with channel widths ranging from (a) 200 μm, (b) 150 μm, (c) 100 μm, (d) 30 μm, (e) 25 μm at low magnification and (f) 25 μm at high magnification. The results show that some uneven profiles are clearly found in all embossed ribs and even some wrinkles are formed in the smaller ribs (**Figure 7**d-f). These results are generally similar to the filling results in CG pure Al.[9] The dual phases can be identified on the surfaces of the embossed ribs, and there are prominent effects on the formation of the wrinkle profiles in the embossed ribs of widths of less than 100 μm. Thus, the co-existence of the α and β phases brings about an adverse filling quality in the micro-embossing process of the CG dual-phase alloy.

Figure 8 shows the surface topographies of the micro-ribs after micro-embossing of the UFG dual-phase alloy with channel widths of (a) 200 μm, (b) 150 μm, (c) 100 μm, (d) 50 μm, (e) 25 μm with low magnification and (f) 25 μm with high magnification. It is clear that the folds on the rib surfaces have almost disappeared and the surface quality of the embossed ribs is significantly improved using the UFG dual-phase alloy compared with the ribs of the CG dual-phase material, and this is true especially when the channel width is small. Careful inspiration of **Figure 8**e shows that obvious α phase and α+β phases are observed on the top surface and these different phases have no effect on the formability of the embossed rib which is different from the CG dual-phase alloy shown in Fig. 7(f). The results show also that the co-existence of the α and β phases along the width direction has little effect on the surface quality of the embossed ribs for the UFG dual-phase alloy.

3.3 Microstructure observations after micro-embossing in the dual-phase Mg-Li alloy

To further investigate the filling behavior, the microstructures of the cross-sections in the embossed ribs were observed for the CG and UFG dual-phase Mg-Li alloys. For the CG material, the cross-sectional shapes of the embossed ribs approach a regular rectangle with increasing channel width (**Figure 9**). When the channel widths are greater than ~150 μm, the surface profiles of the embossed ribs are regular and the hard α phase has a slight protuberance on the upper surface of the embossed rib due to the co-existence of both α and β phases as shown in **Figure 9**a and b. With a further decrease in channel width, the upper surface of the embossed rib is more uneven due to the co-existence of the α and β phases as shown in **Figure 9**c and d which contrasts with **Figure 9**a and b. When the α and β phases are in contact with the side wall, inhomogeneous deformation takes place and pits are observed

on the side walls of the embossed ribs due to the co-existence of the α and β phases. When the channel width decreases to 25 μm, there is only a single phase in the width direction of the rib in some positions as shown in **Figure 9**e. For this situation, the filling behavior is similar to a single crystal filling so that the cross-sectional shape of the rib becomes trapezoid and the side walls of the rib no longer cling to the die. This is because the deformation is mainly dependent upon slip within the grains which leads to a large number of dislocations and uneven deformation in different regions in the grain under a single crystal filling. Simultaneously, the side wall of the rib no longer clings to the die and the cross-sectional shape becomes trapezoid as shown in **Figure 9**e.

For the UFG dual-phase alloy, the surface profile of the embossed ribs is more regular with smooth upper surfaces and side walls compared with the CG alloy as shown in **Figure 10** for widths of (a) 200 μm, (b) 150 μm, (c) 100 μm, (d) 50 μm and (e) 25 μm. Thus, when the channel width is greater than 50 μm the surface profile of the embossed ribs is regular and exhibits good symmetry. However, for a channel width of 25 μm the upper surface of the embossed rib is biased to one side as shown in **Figure 10**e and has an improved contour profile compared with **Figure 9**e. These results reveal that the embossed ribs of the UFG dual-phase alloy have regular and smooth contour profiles compared with the CG dual-phase alloy due to the distributions of the different phases for the UFG alloy. The results are fully consistent with the SEM results shown earlier in section 3.2.

3.4 Finite element simulations during micro-embossing in the dual-phase Mg-Li alloy

The simulation results are depicted in **Figure 11** and **Figure 12** for the CG and UFG dual-phase alloys, respectively. For the CG alloy in **Figure 11**, the severe deformation zone is near

the fillet of the rib roots where the equivalent strain and the equivalent stress are larger than in other areas during the filling process. In addition, the deformation behavior of the α and β phases is different where the equivalent stress is larger and the equivalent strain is less for the α phase compared with the β phase. In practice, the calculated equivalent strain exhibits a butterfly-like profile as shown in **Figure 11**c. These simulated results reveal that the deformation of both sides of the rib is uneven due to the co-existence of the α and β phases where these two phases have different mechanical properties in terms of hardness and strength.

For the UFG dual-phase alloy, the simulated results are consistent with the CG dual-phase alloy where the severe deformation zone is near the fillet of the rib roots and the equivalent strain and equivalent stress are larger than in other areas during the filling process as shown in **Figure 12**. Nevertheless, there is little difference during micro-embossed processing and the equivalent strain does not present a butterfly-like configuration compared with the CG alloy. In addition, the deformation including equivalent stress and equivalent strain on both sides of the rib is symmetrical and the co-existence of a α phase and a β phase has little or no influence compared to the CG alloy. These simulated predictions are therefore consistent with the experimental results.

4. Discussion

4.1 Micro-embossing formability of dual-phase Mg-Li alloy at ambient temperature

The formability of micro-embossing is a significant issue that determines whether a selected material has the potential for use in applications in the field of micro-forming processes. Previous studies demonstrated that the formability is affected in practice by the characteristic dimensions of the female die and the grain sizes of the materials.[35] A major objective of the

present research was to evaluate and compare the formability of micro-embossing in CG and UFG dual-phase Mg-Li alloys at ambient temperature. The filling height data indicate that the height of the filled rib increases with increasing channel width in both the CG and UFG alloys (**Figure 6**). Nevertheless, the rate of filling height increase for the UFG alloy is lower than for the CG alloy. In addition, the filling height of the rib for the CG alloy is significantly higher than for the UFG alloy after micro-embossing with a selected size of female die. Accordingly, these results demonstrate that a larger embossing force is required to obtain a high filling height in micro-embossing for UFG metals at ambient temperature.

To evaluate the influence of grain size and tool dimensions on the formability, the relationship between the ratio of the embossed rib height to width, *h/w*, and the ratio of the female die width to the grain size, *w/d*, are summarized in **Figure 13** from the results in **Figure 6** for (a) the CG alloy and (b) the UFG alloy. The results show that the ratio, *h/w*, significantly increases with a decrease in the ratio w/d and these results indicate that grain size and tool dimensions have complicated interactive influences on the formability of micro-embossing under the same force at ambient temperature. It can be shown that a larger channel width in a female die is beneficial in improving the formability of micro-embossing for the CG alloy compared with the UFG alloy. Furthermore, the poorer filling height in micro-embossing at ambient temperature for the UFG alloy is attributed to the higher mechanical properties caused by the smaller grains. These results reveal that a higher embossing force is required to obtain a high filling height of micro-embossing for the UFG metals at ambient temperature.

Surface topography and microstructural observations of the sample cross-sections reveal that the embossed ribs of the UFG alloy have improved surface quality and more regular

profiles by comparison with the CG alloy. Some uneven profiles were observed in all embossed ribs and even some wrinkles were formed in the smaller ribs for the CG alloy as shown in **Figure 7**. By contrast, the folds on the rib surfaces almost disappeared for the UFG alloy especially when using a small channel width as shown in **Figure 8**. From the results in **Figure 9** and **Figure10**, it can be seen that the upper surfaces and the profiles of the ribs are more smooth and regular for the UFG specimens compared with the CG specimens. Further careful inspiration shows also that the effect on the formality of the different phases in the dual-phase Mg-Li alloy is less for the UFG structure compared with the CG structure. Consequently, the results provide a clear demonstration that the co-existence of the α and β phases has less effect on the surface quality of the embossed ribs for the UFG alloy than for the CG alloy. Similar predictions were also obtained by numerical simulation. Based on these results, it may be concluded that the micro-embossing formability of the UFG alloy is better than for the CG alloy due to the minor influence of the dual phases on the formability of the UFG material.

4.2 Deformation mechanism of micro-embossing in the dual-phase Mg-Li alloy

The experimental and numerical modeling results demonstrate that the different phases of the dual-phase Mg-Li alloy have a significant effect on the deformation of the micro-embossing compared with the pure material. Furthermore, the grain size also has an effect on the deformation of micro-embossing

For the CG alloy, when the channel width is 25 or 50 μm, the grain size of the CG specimen is close to the channel width so that only one or two grains deform during the processing of micro-embossing and this leads to a non-uniform deformation in the grain

interiors and a consequent poor compatibility of deformation between adjacent grains. The co-existence of α and β phases causes a filling behavior that is different due to the differences in the mechanical properties of these two phases such as in microhardness and strength. These two aspects produce a poor surface quality with serious folding during the micro-embossing for the CG material with a small channel width. When the channel width is larger than 100 μm, the folds caused by inhomogeneous deformation between the different grains and phases are greatly relieved. Thus, the main cause of inhomogeneous deformation on different positions of the embossed ribs is the co-existence of these α and β phases. By contract, for the UFG alloy the influence of the co-existence of these two phases on the filling properties during micro-embossing is less than with the CG alloy. This difference is mainly because the distributions of the α and β phases becomes reasonably uniform after HPT. The average grain size of the UFG alloy after HPT is ~290 nm which is far smaller than the channel width and this means a large number of grains are deformed during the micro-embossing processing where the compatibility of deformation between adjacent grains is greatly improved. Based on these two aspects, the folds caused by inhomogeneous deformation between different grains and phases almost disappear for the UFG alloy. The cross-sectional microstructures of the micro-embossed ribs shown in Figs 9 and 10 and the simulation results shown in **Figure 11** and **Figure 12** both lead to the same overall conclusions.

4.3 The potential for using the UFG Mg-Li alloy in micro-forming applications

An important objective of this research was to evaluate the potential applications of the UFG dual-phase Mg-Li alloy in the fabrication of micro-forming. The influence of grain size on material flow behavior and formability is much greater in micro-forming, especially because

of size effects when the processing is scaled down from conventional levels to dimensions at the micro-level. In particular, grain size effects may lead to an inhomogeneous material performance which produces inaccuracies in the processed shape and introduces scatter in the subsequent properties of the product. This was demonstrated recently for a UFG pure Al processed by ECAP which was successfully utilized for the micro-forming of micro-turbine parts.[38] The present study with a Mg-Li alloy has shown that the surface quality of embossed ribs for the UFG alloy is better than for the CG alloy, especially when the channel width is small. In addition, the adverse effects of dual phases on the formability of micro-embossing are reduced significantly for the UFG alloy and there is good surface quality and a regular counter profile compared with the CG alloy. The current results demonstrate that the UFG alloy can be micro-formed with high quality without any adverse effect of different phases, especially with smaller shape sizes.

Figure 14 shows the surface topography of embossed micro-channel arrays on the UFG alloy at ambient temperature with channel widths ranging from (a) 50 μm, (b) 100 μm, (c) 150 μm and (d) 200 μm. From these images, it can be seen that the embossed micro-channel arrays with different widths are all very well embossed with good geometrical transferability and with the introduction of no obvious disfigurements using the UFG alloy. Therefore, it is recommended that the UFG dual-phase alloy processed by HPT has a very good potential for use in applications involving micro-forming.

5. Conclusions

(1) In experiments on a dual-phase Mg-Li alloy it is shown that the height of the embossed ribs of the alloy increases with increasing channel width for both coarse-grained

(CG) and ultrafine-grained (UFG) specimens. The surface quality improves gradually with an increase in the channel width. For the CG alloy, the embossed ribs have a poor surface quality with folding, especially when the channel width is small. By contrast, a high surface quality of embossed ribs is obtained using a UFG alloy at different widths of the channel.

(2) The co-existence of the α and β phases influences the deformation processing of micro-embossing. For the CG alloy the different mechanical properties of the α and β phases lead to a minor α phase protuberance on the upper surface of the embossed rib during the deformation processing whereas for the UFG alloy this phenomenon is not observed.

(3) Simulations using different mechanical properties for the dual phases demonstrate consistency with the experimental results. The simulation results show the severe deformation zone is near the fillet of the embossed rib roots where the equivalent strain and equivalent stress are larger than in other areas during the micro-embossing. The deformation of both sides of the rib is uneven for the CG material but the equivalent stress and equivalent strain of both sides of the rib are symmetrical for the UFG material.

(4) Micro-channel arrays using the UFG alloy with channel widths ranging from 50 to 200 μm at ambient temperature produced by micro-embossing are all embossed well with good geometrical transferability and no obvious disfigurement. The results demonstrate that the UFG alloy processed by HPT has a very good potential for applications in micro-forming.

Acknowledgement

This work was supported by the National Natural Science Foundation of China under Grants No. 51635005 and No. 51475124. Partial support was provided by the 111 Project under

Grant No. B18017 and the Postdoctoral Scientific Research Developmental Fund of Heilongjiang Province under Grant No. LBH-Q15039.

Conflict of Interest

The authors declare no conflict of interest.

Keywords

dual-phase microsructures, high-pressure torsion, Mg-Li alloy, micro-embossing, micro-forming

Received: ((will be filled in by the editorial staff))
Revised: ((will be filled in by the editorial staff))
Published online: ((will be filled in by the editorial staff))

[1] X.G. Qiao, M.T. Bah, J. Zhang, N. Gao, Z. Moktadir, M. Kraft, M.J. Starink, *J. Micromech. Microeng.* **2010**, 20, 105002.

[2] H. Ottevaere, S.V. Overmeire, J. Albero, L. Nieradko, G. Desmet, C. Gorecki, H. Thienpont, *Microfluid. Nanofluid.* **2015**, 18, 559.

[3] Z. Liu, Y. Yi, H. Xu, X. Zhang, T.H. Ngo, M. Smet, *Adv. Mater.* **2010**, 22, 2689.

[4] M.W. Fu, W.L. Chan, *Int. J. Adv. Manuf. Technol.* **2013**, 67, 2411.

[5] R. Neugebauer, A. Schubert, J. Kadner, T. Burkhardt, *Adv. Technol. Plast.* **1999**, 2, 19.

[6] T. Otto, A. Schubert, J. Böhm, T. Gessner, *Proc. SPIE* **2000**, 4179, 96.

[7] J. Böhm, A. Schubert, T. Otto, T. Burkhardt, *Microsyst. Technol.* **2001**, 7, 191.

[8] J. Jiang, F. Mei, W.J. Meng, G.B. Sinclair, S. Park, *Microsyst. Technol.* **2008**, 14, 815.

[9] J. Xu, L. Shi, C.X. Wang, D.B. Shan, B. Guo, *J. Mater. Process. Technol.* **2015**, 225, 375.

[10] F. Vollertsen, D. Biermann, H.N. Hansen, I.S. Jawahir, K. Kuzman, *CIRP Ann. Manuf. Technol.* **2009**, 58, 566.

[11] W.L. Chan, M. W. Fu, B. Yang, *Mater. Des.* **2011**, 32, 3772.

[12] W.L. Chan, M.W. Fu, Mater. Sci. Eng. A. **2011**, 528, 7674.

[13] X.W. Wang, J. Xu, D. Shan, B. Guo, J. Cao, *Mater. Des.* **2017**, 127, 134.

[14]R. Zhao, J.Q. Han, B.B. Liu, M. Wan, *Mater. Des.* **2016**, 94, 195.

[15] G.Y. Kim, M. Koc, J. Ni, *ASME Conf. Proc.* **2006**, 277.

[16] G.Y. Kim, M. Koc, J. Ni, *J. Manuf. Sci. Eng. – Trans. ASME* **2008**, 130, 041017.

[17] W.L. Chan, M.W. Fu, *Mater. Sci. Eng. A.* **2012**, 556, 60.

[18]C.J. Wang, D.B. Shan, J. Zhou, B. Guo, L.N. Sun, *J. Mater. Process. Technol.* **2007**, 187, 256.

[19]G.C. Wang, W. Zheng, T. Wu, H. Jiang, G.Q. Zhao, D.B. Wei, Z.Y. Jiang, *J. Mater. Process. Technol.* **2012**, 212, 678.

[20] Z.Y. Gao, L.f. Peng, P. Y. Yi, X.M. Lai, *J. Mater. Process. Technol.* **2015**, 219, 28.

[21]X. Meng, R. Wu, M. Zhang, L. Wu, C. Cui, *J. Alloy. Compd.* **2009**, 486, 722.

[22]R. Wu, Y. Yan, G. Wang, L.E. Murr, W. Han, Z. Zhang, M. Zhang, *Int. Mater. Rev.* **2014**, 60, 65.

[23]I. Shin, E.A. Carter, *Acta Mater.* **2014**, 64, 198.

[24] Y. Yang, X. Xiong, J. Su, X. Peng, H. Wen, G. Wei, F. Pan, E.J. Lavernia, *J. Alloy. Compd.* **2018**, 750, 696.

[25] Y. Zou, L. Zhang, H. Wang, X. Tong, M. Zhang, Z. Zhang, *J. Alloy. Compd.* **2016**, 669, 72.

[26]G. H. Park, J. T. Kim, H. J. Park, Y. S. Kim, H. J. Jeong, N. Lee, Y. Seo, J. Y. Suh, H. T. Son, W. M. Wang, J. M. Park, K. B. Kim, *J. Alloy. Compd.* **2016**, 680, 116.

[27]T.B. Massalski (Ed.), *Binary Alloy Phase Diagrams*, ASM, Metals Park, OH **1986**.

[28] Y. Zou, L. Zhang, Y. Li, H. Wang, J. Liu, P. Liaw, H. Bei, Z. Zhang, *J. Alloy Compt.* **2018**, 735, 2625.

[29]X. Liu, R. Wu, Z. Niu, J. Zhang, M. Zhang, *J. Alloy Compt.* **2012**, 541, 372.

[30]M. Furui, C. Xu, T. Aida, M. Inoue, H. Anada, T.G. Langdon, *Mater. Sci. Eng. A.* **2005**, 410-411, 439.

[31]M. Furui, H. Kitamura, H. Anada, T.G. Langdon, *Acta Mater.* **2017**, 55, 1083.

[32]H. Matsunoshita, K. Edalati, M. Furui, Z. Horita, *Mater. Sci. Eng. A.* **2015**, 640, 443.

[33]K. Edalati, T. Masuda, M. Arita, M. Furui, X. Sauvage, Z. Horita, R.Z. Valiev, *Sci. Rep*. **2017**, 7, 2662.

[34]J. Xu, M. Shirooyeh J. Wongsa-Ngam, D. Shan, B. Guo, T.G. Langdon, *Mater. Sci. Eng. A.* **2013**, 586, 108.

[35]J. Xu, X. Wang, M. Shirooyeh, G. Xin, D. Shan. B. Guo, T.G. Langdon, *J. Mater. Sci.* **2015**, 50, 7424.

[36]R.B. Figueiredo, P.R. Cetlin, T.G. Langdon, *Mater. Sci. Eng. A* **2011**, 528, 8198.

[37] W.L. Chan, M.W. Fu, J. Lu, *Mater. Des.* **2011**, 32, 525.

[38]J. Xu, X. Zhu, D. Shan, B. Guo, T.G. Langdon, *Adv. Eng. Mater.* **2015**, 636, 352.

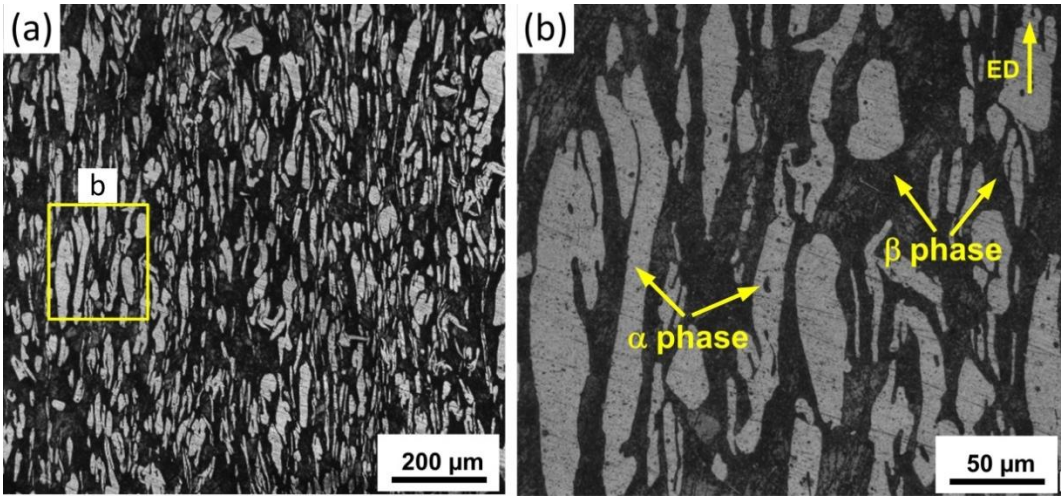

Figure 1. Microstructure of the as-received Mg-Li alloy at (a) lower and (b) higher magnifications.

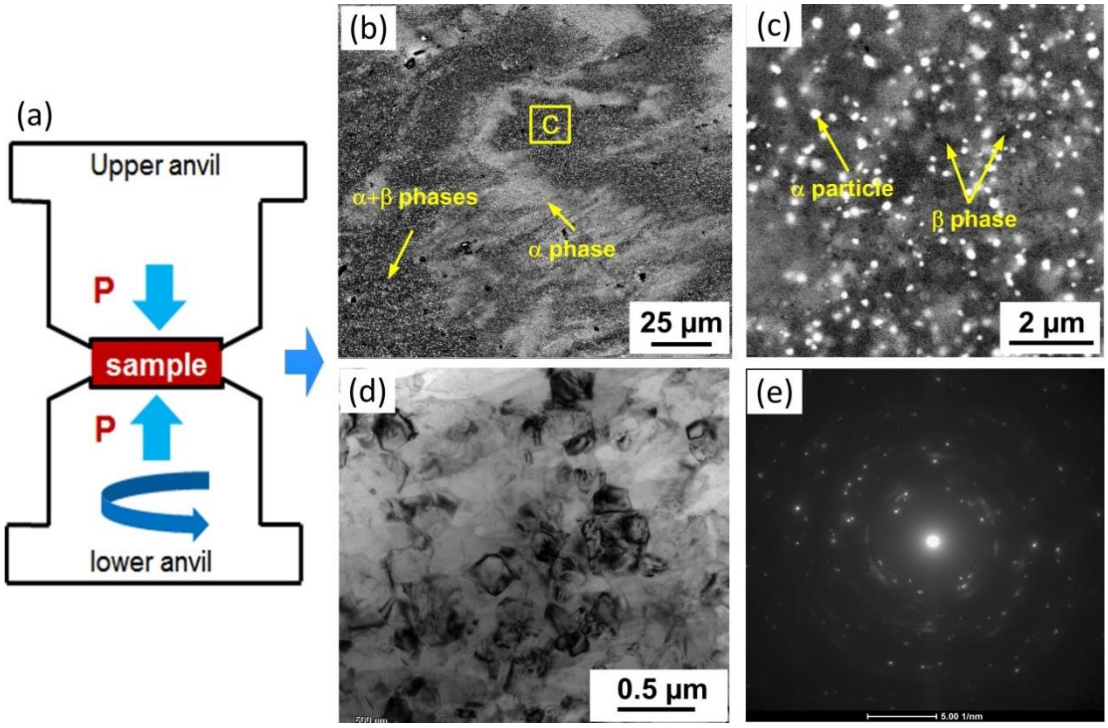

Figure 2 (a) Schematic diagram of HPT processing for UFG dual-phase Mg-Li alloy, (b) SEM image at low magnification, (c) SEM image at high magnification, (d) TEM image and (d) diffraction pattern.

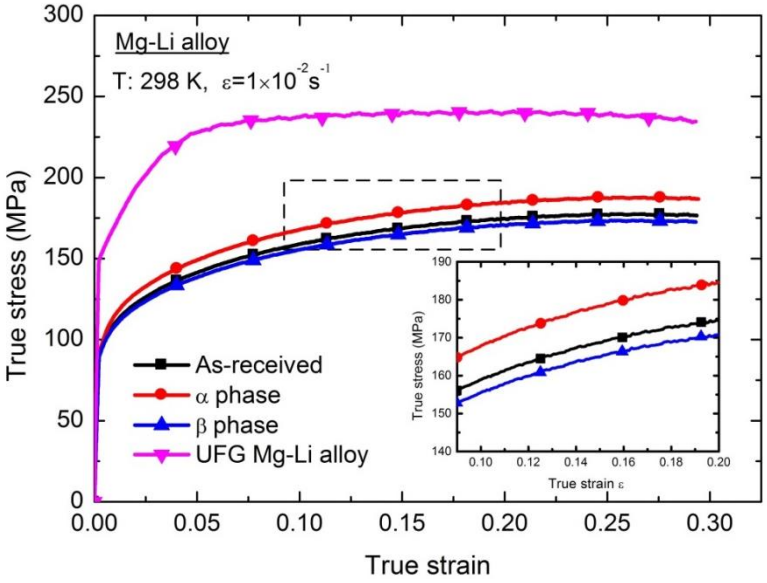

Figure 3 True stress-true strain curves for CG and UFG dual-phase Mg-Li alloys.

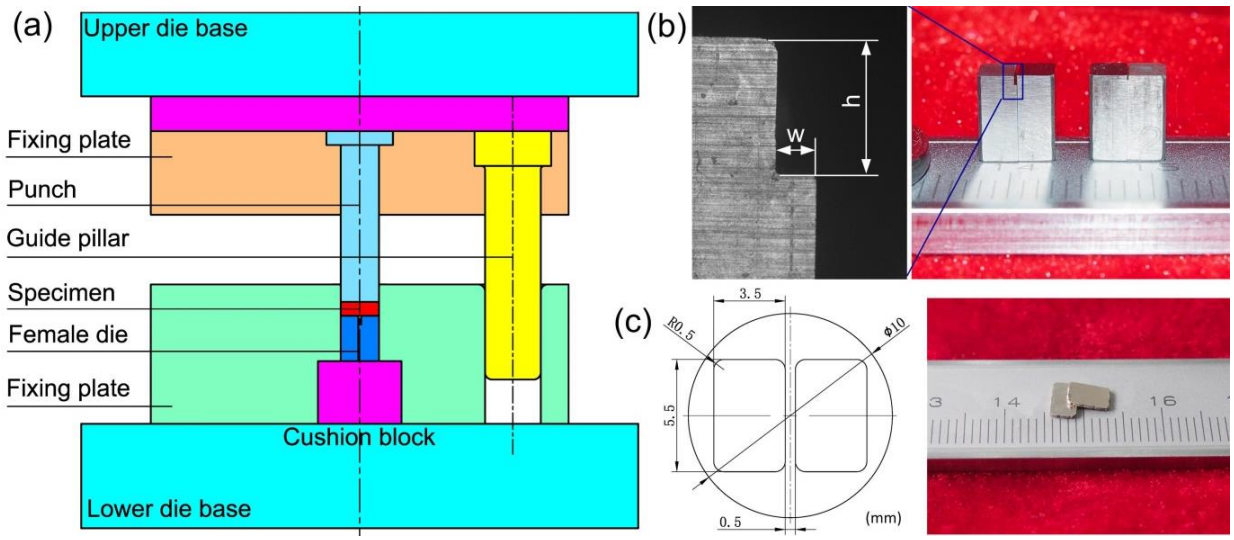

Figure 4 (a) Schematic diagram of micro-embossing tool, (b) female die and (c) micro-embossing samples.

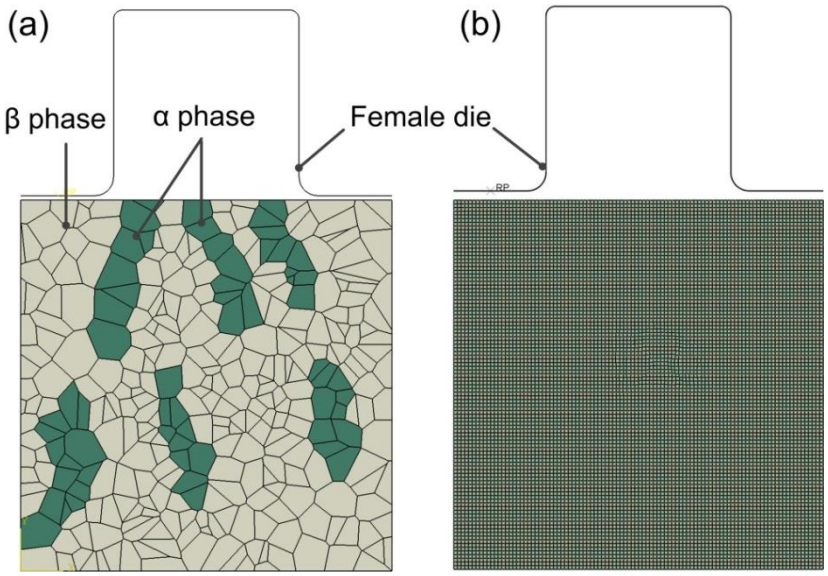

Figure 5 Finite element model for micro-embossing of (a) CG and (b) UFG dual-phase alloy.

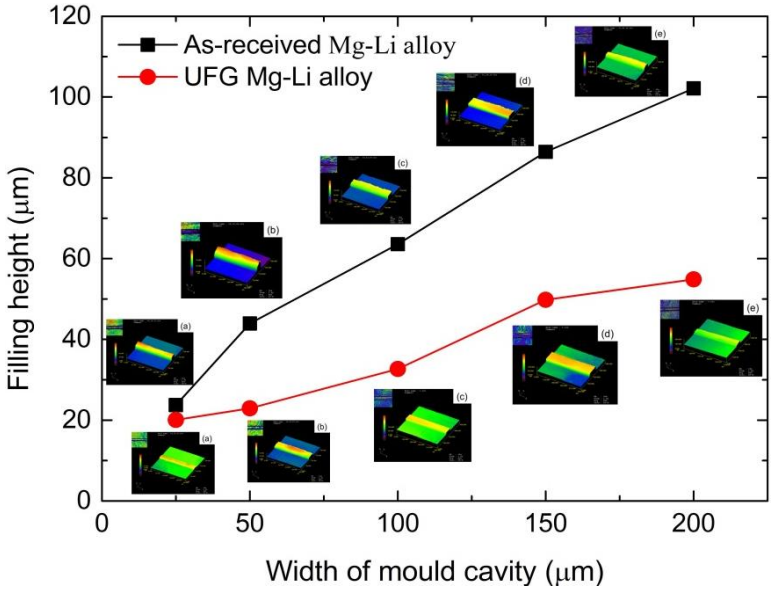

Figure 6 Filling height of dual-phase Mg-Li alloy with different widths of channel.

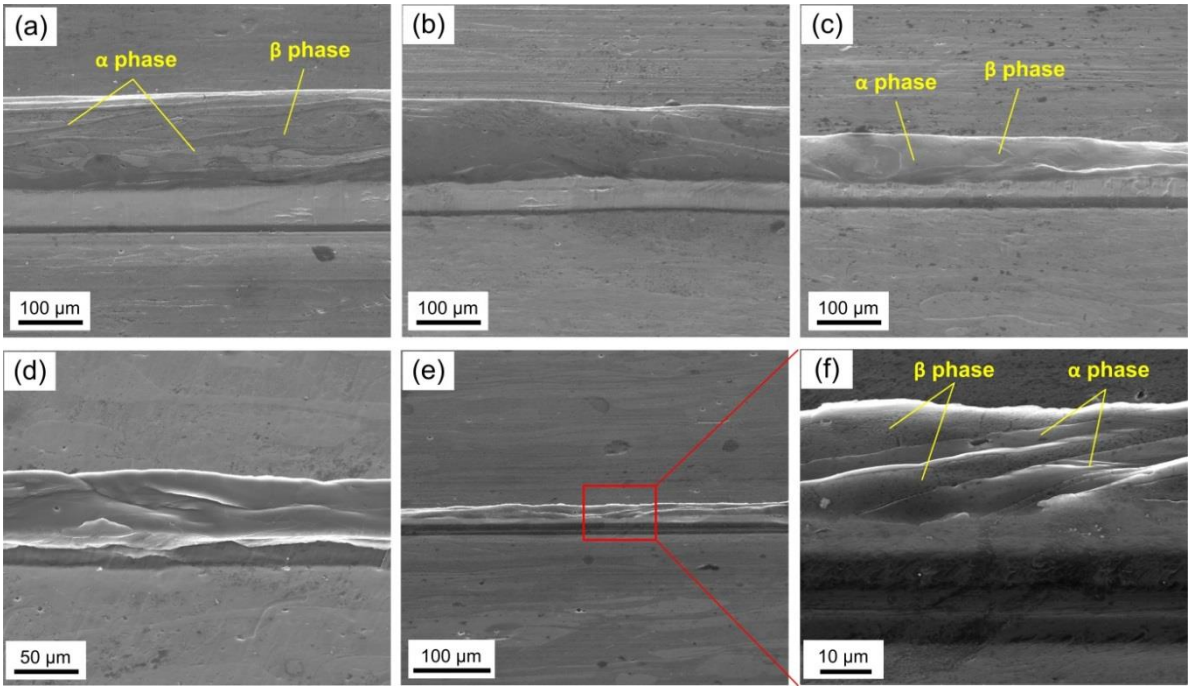

Figure 7 SEM images of micro-embossed ribs with widths of (a) 200 μm, (b) 150 μm, (c) 100 μm, (d) 50 μm, (e) 25 μm with low magnification and (f) 25 μm with high magnification using CG alloy.

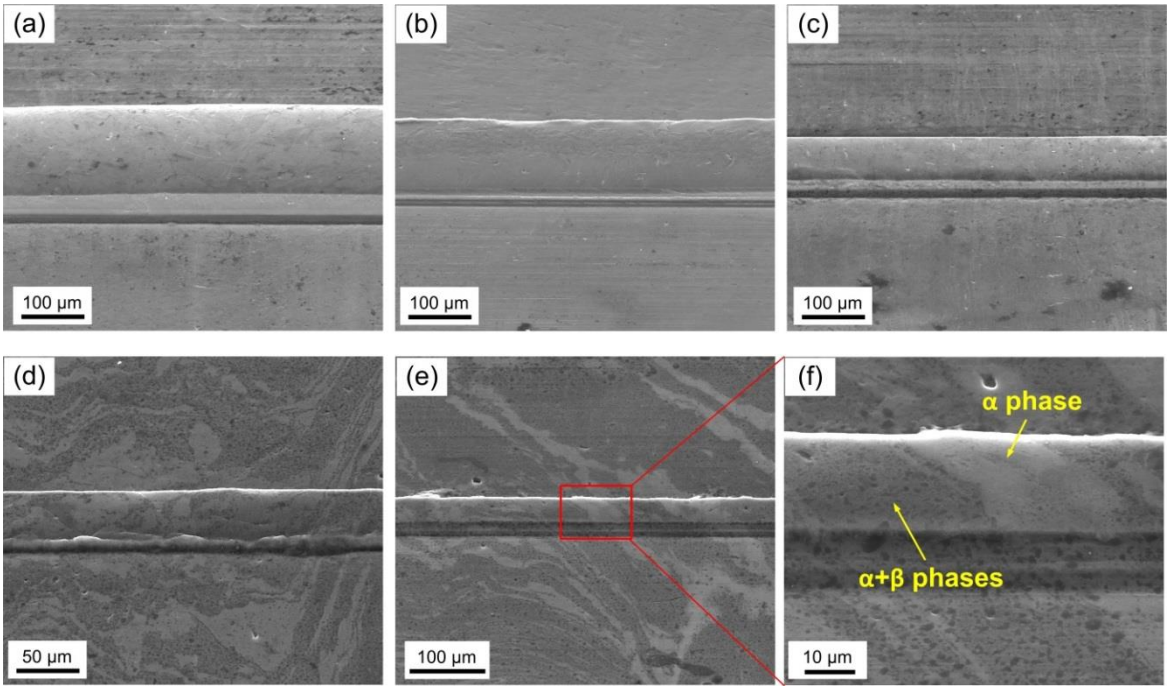

Figure 8 SEM images of micro-embossed ribs with widths of (a) 200 μm, (b) 150 μm, (c) 100 μm, (d) 50 μm, (e) 25 μm with low magnification and (f) 25 μm with high magnification using UFG alloy.

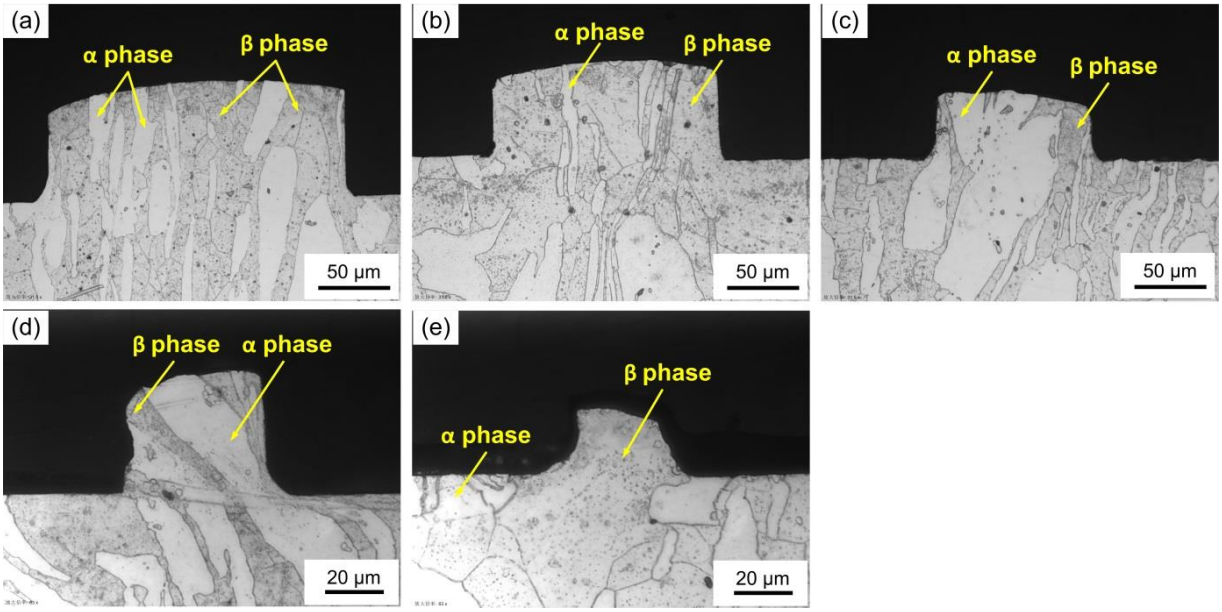

Figure 9 Cross-section microstructures of micro-embossed ribs with widths of (a) 200 μm, (b) 150 μm, (c) 100 μm, (d) 50 μm and (e) 25 μm using CG alloy.

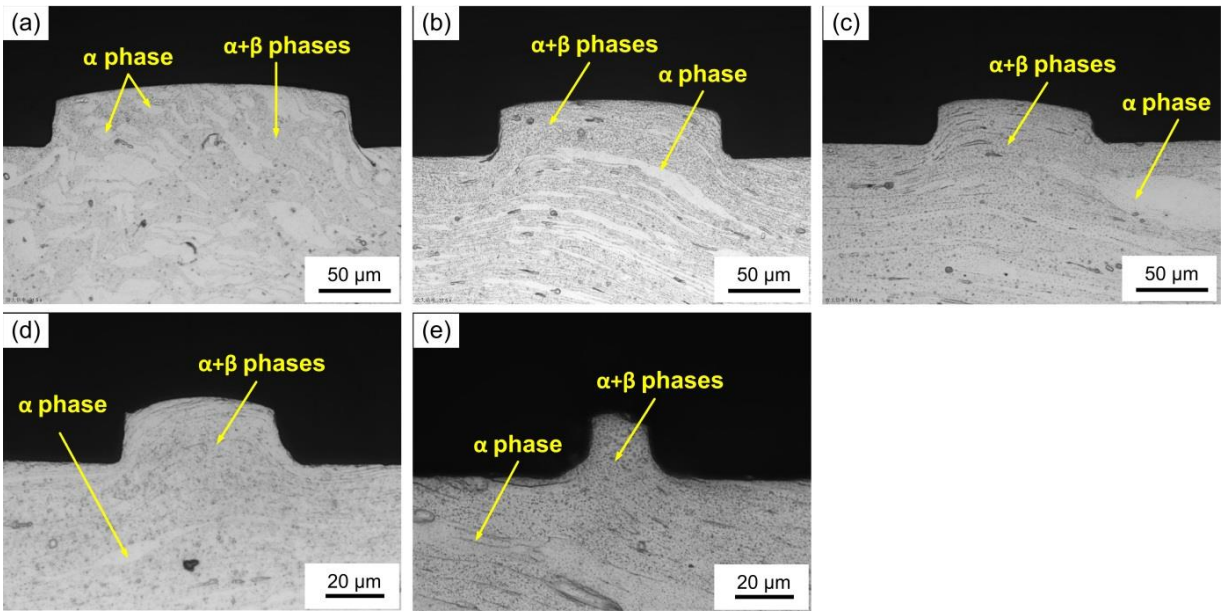

Figure 10 Cross-section microstructures of micro-embossed ribs with widths of (a) 200 μm; (b) 150 μm; (c) 100 μm; (d) 50 μm and (e) 25 μm using UFG alloy.

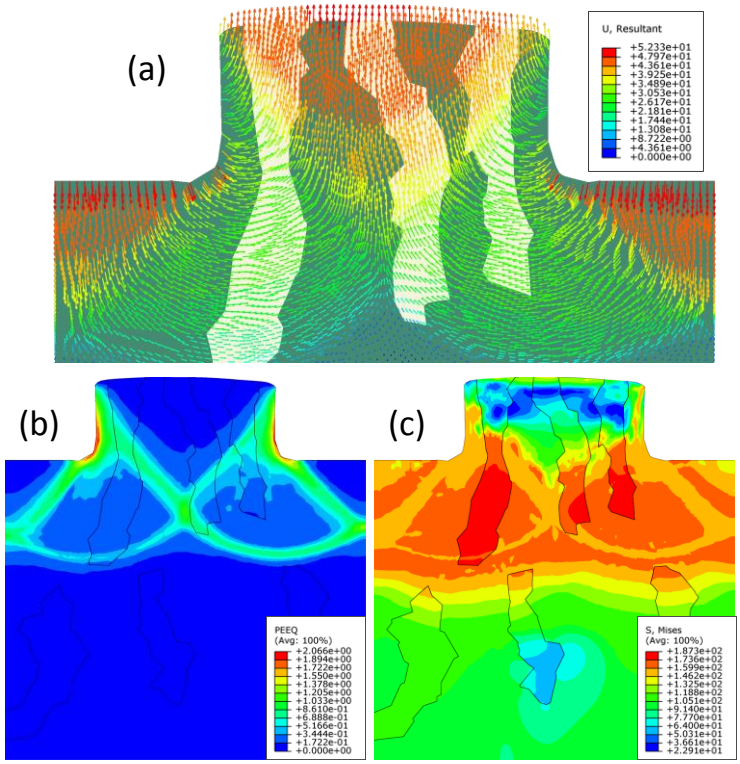

Figure 11 The simulated results of (a) the displacement vector, (b) the equivalent stress and (c) the equivalent strain for the CG alloy.

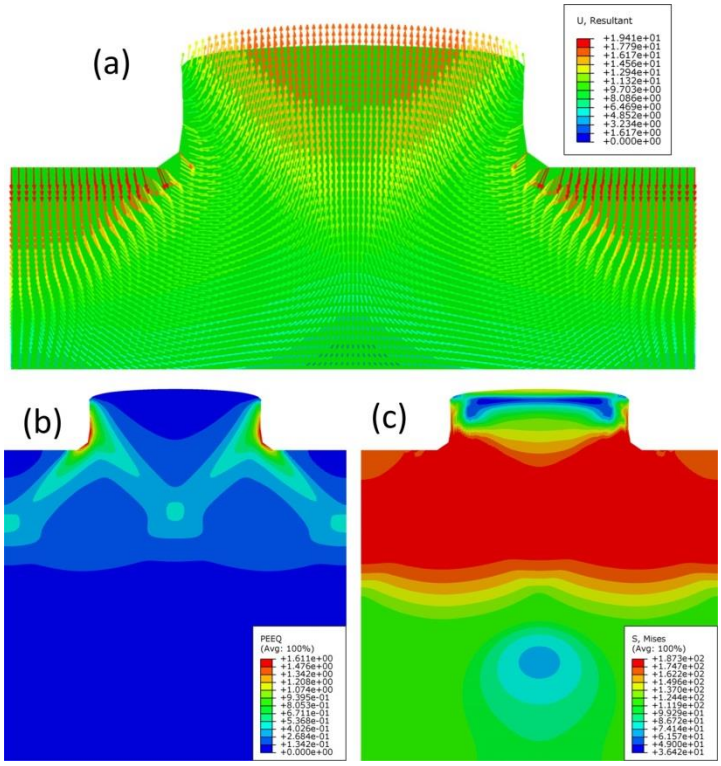

Figure 12 The simulated results of (a) the displacement vector, (b) the equivalent stress and (c) the equivalent strain for the UFG alloy.

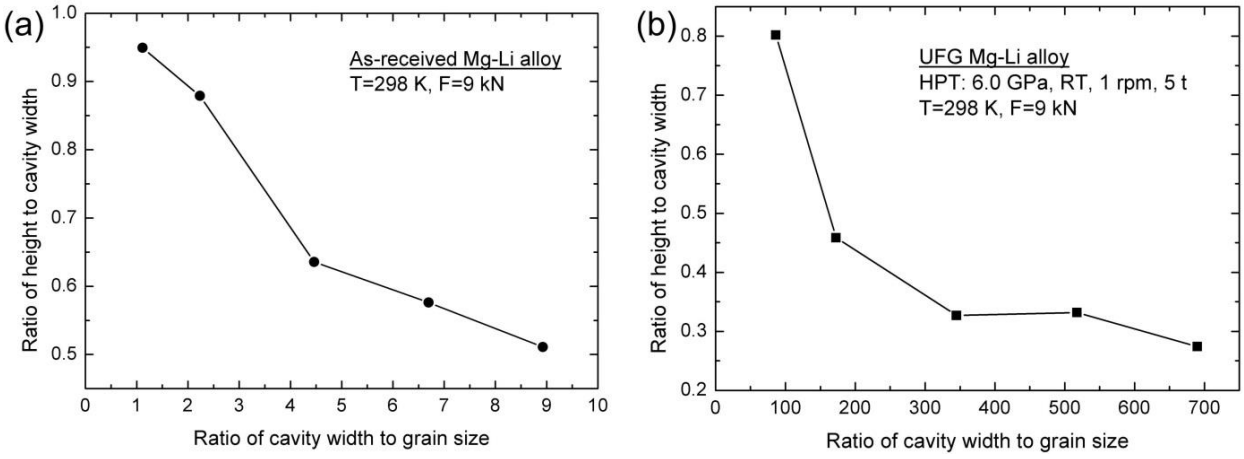

Figure 13 The relationship between the ratio of the embossed rib height to width and the ratio of the cavity width to grain size for (a) the CG and (b) the UFG alloys.

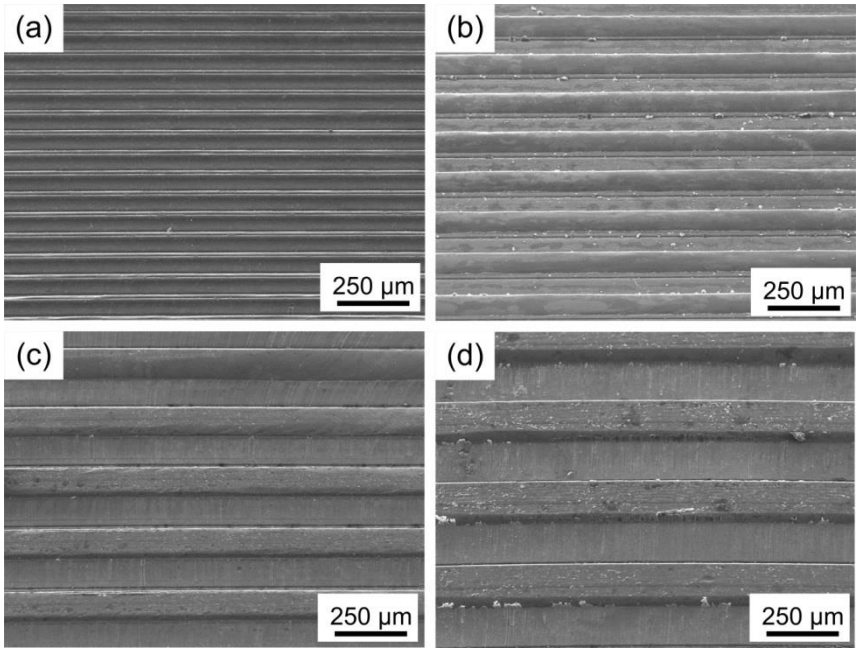

Figure 14 SEM images of the micro-array channels with widths of (a) 50 μm, (b) 100 μm, (c) 150 μm and (d) 200 μm using the UFG alloy.

In this paper, the interactive effects of cavity widths and dual phases on the formability of micro-embossing were analyzed which shows that the UFG Mg-Li alloy reduces the adverse effects of dual phases on the formability of micro-embossing compared with CG materials. Meanwhile, results demonstrate that the UFG alloy processed by HPT has potential applications in micro-forming.